Novel wear-resistant anti-bacterial stainless steel surfaces

Tian, Linhai; Li, Xiaoying; Dong, Hanshan

DOI:
10.1080/02670844.2017.1316453

Novel Wear-Resistant Anti-Bacterial Stainless Steel Surfaces

Linhai Tian[1, 2*], Xiaoying Li[1] and Hanshan Dong[1]

[1] School of Metallurgy and Materials, University of Birmingham, Birmingham B15 2TT, UK

[2] Research Institute of Surface Engineering, Taiyuan University of Technology, Taiyuan 030024, China

Abstract

To generate a long-lasting antibacterial surface on stainless steels for demanding applications involving rubbing and wear, a novel triple-glow plasma (TGP) technology was employed to generate Ag/N co-alloying layers on AISI 316 austenitic stainless steel. The mechanical, chemical, antibacterial and tribological behaviour of the samples treated under different settings and parameters were fully characterised. It is identified that a durable antibacterial surface has been achieved using the novel triple-glow plasma technology under an optimal parameters, as proved by the high hardness, low wear rate and high antibacterial efficacy. A bilayer structure composed of a thin top layer containing about 20-25% Ag embedded in N supersaturated austenite followed by a relatively thick (~10 μm) S-phase layer was formed after Ag/N co-alloying by TGP. The silver embedded in the hard S-phase provides bactericidal activity against Gram-positive *Staphylococcus aureus* (*S. aureus*) with a reduction rate of 95% compared with the untreated stainless steel.

Keywords: AISI316; antibacterial; silver; triple-glow plasma

* L Tian carried out this research in University of Birmingham, and now back to China.

1 Introduction

Austenitic stainless steels are important metallic biomaterials for medical devices owing to their attractive combination of excellent corrosion resistance, good mechanical properties, high resistance to repeated sterilisation and adequate biocompatibility, coupled with their outstanding formability and cost-effectiveness. Hence, austenitic stainless steels are the material of choice for bone fixation devices, body implants, surgical and dental tools and instruments and hospital facilities [1]. Austenitic stainless steels are also commonly used in the food processing industry.

Although all these surgical and dental tools and instruments have greatly contributed to enhanced quality of life, they have also been a major cause of infections since some transmissible agents (such as bacteria and prions) may not be destroyed by normal sterilisation procedures and cross-contamination may occur when handling these medical devices [2]. Indeed, how to combat multi-resistant bacteria has become one of the greatest challenges in the treatment of post-operative infections. For example, external fracture fixation is a method used to treat fractures that are severely comminuted or open to the environment. The most common complication in stainless steel external fixation systems is pin tract infection with infection rates ranging from 2% to as high as 30% [3]. This is because the site of entry of the pin is constantly open and cannot heal and hence presents a critical interface between the external stainless steel pin and internal muscle and bone. The consequences of infected pin sites include pin loosening, fracture destabilisation and osteomyelitis, thus leading to additional surgical antibiotic interventions and poor/slow healing [4].

In addition, outbreaks of hospital-acquired infections (HAI) are frequently reported [5] and contamination of environmental surfaces in hospital rooms plays an important role in the transmission of several key pathogens. These include methicillin-resistant *Staphylococcus* aureus (MRSA), vancomycin-resistant *Enterococcus* species (VRE), *Clostridium* difficile, *Acinetobacter* species, and noroviruses [6]. For example, within the EU, over 4 million patients contract a hospital acquired infection (HAI) each year, which accounts for an estimated 37,000 deaths. In the USA, about five percent of patients admitted to hospitals get HAIs, adding $45 billion to the annual cost of healthcare [7]. It is reported that there are 300,000 cases of HAIs annually in the UK with 5,000 deaths and >£1bn loss to the NHS [8].

Antibacterial or self-disinfecting surfaces have progressively become a primary strategy in the fight against medical device-associated and hospital-acquired infections despite the achievement made during the past decades in terms of aseptic techniques, control of environment sterility, and perioperative antibiotic prophylaxis [9]. One widely available approach is to impregnate or coat medical device surfaces with a germicide but this has the potential to lead to bacteria developing resistance to the germicide and to clinically useful antibiotics [10].

It is well-known that surface characteristics are crucial for effective prevention of bacterial colonisation, and hence surface engineering, via surface modification or surface coating, is intensively researched to generate antibacterial or self-disinfecting surfaces. For example, surface micro-topographical features and surface wettability can be modified by roughening (such as shot-peening and grinding) or micro-patterning (micro-contact printing and laser-patterning) to effectively influence bacterial cell adhesion [11 12]. However, the durability of such micro-topographical features for bio-tribological applications is of concern. Alternatively, antibacterial or self-disinfecting surfaces can be created by modifying or coating surfaces with silver since silver and its compounds are some of the strongest bactericides by the denaturing of thiol groups of bacterial proteins and enzymes [13]. Silver, one of the strongest bactericides, has been extensively researched and as a result has found some important applications due to its desirable combination of a broad-spectrum of antimicrobial activities and its remarkably low human toxicity. As a useful disinfectant, nano particulate silver is added into PMMA bone cement [14] and silver-containing substance are also applied to medical devices such as indwelling catheters and wound dressings [15].

Currently there are two surface engineering approaches to introduce silver and its compounds to the surface of austenitic stainless steels: (1) coating the surfaces with pure Ag or Ag containing composites and (2) alloying the surfaces with Ag. The first approach, silver-containing coatings, is the most widely researched method. For instance, Ag-doped polymer coating and pure Ag are used to coat stainless steel surfaces. However, these coatings are relatively soft and hence their durability is poor for tribological applications. Moreover, it has also been reported that no statistically significant difference could be observed in the clinical outcomes of Ag-coated and uncoated steel fixation pins [16]. Some attempts have been made to develop Ag-containing nanocomposite coatings with increased hardness [4] but ensuring adequate bonding between the coating and the substrate is always a challenge for tribological applications.

In the second approach, the authors have, in the past five years, endeavoured to generate durable anti-bacterial stainless steel surfaces by developing advanced plasma surface alloying technologies. For example, an advanced active screen plasma co-alloying technology was developed to alloy stainless steel surfaces with both Ag (for antibacterial) and N (for hardening) using a Ag-containing stainless steel screen. The co-alloyed stainless steel surface revealed a high anti-bacterial efficacy but the durability of the anti-bacterial surface is still limited. This is because it is difficult to produce a deep alloyed case with a high amount of substitutional alloying element Ag at a relatively low-temperature due to its low diffusion coefficient [17]. Consequently, an attempt was made to sequentially alloy stainless steel surfaces first with Ag at high-temperature (930°C) in a double-glow plasma furnace and then with N at low-temperature (430°C) in an active-screen plasma furnace [18]. However, the sequential two-processes conducted in two different furnaces not only significantly increased the processing cost and time but also increased the risk for contamination and oxidation during the changeover between the processes.

In short, the inherent technical limitation for the above active screen plasma technology with Ag-containing stainless steel screen is that the chemical composition and in particular the percentage of the anti-bacterial agent is determined solely by the composition of the Ag-containing screen used. Hence, it is impossible to adjust or control the percentage of the anti-bacterial agent in the co-alloyed surface case without changing the screen (which is time consuming and very costly). This technical challenge can be successfully addressed using the recent developed novel triple-glow plasma (TGP) technology [19]. As shown in Figure 1, an additional Ag cathode with separate power source S1 is installed to control the yielding and hence the amount of Ag in the co-alloyed surface case by adjusting the bias on the Ag cathode. Therefore, a thick co-alloyed case on austenitic stainless steel with controllable amount of Ag can be formed at a relatively low temperature. The mechanical, corrosion, antibacterial and tribological behaviour of the Ag/N co-alloyed layer were fully characterised to identify the potential of the novel triple-glow plasma technology for generating long-lasting antibacterial surfaces for demanding applications involving rubbing and wear (such as surgical tools and orthopaedic implants).

2 Materials and Methods

2.1 Substrate material

Commercial AISI 316 stainless steel with the chemical composition (wt.%.): 0.06 C, 17.20 Cr, 11.70 Ni, 2.2 Mo, 1.3 Mn, and Fe balance was used as the substrate material in this study. Samples of 5 mm in thickness were cut from a hot rolled one inch (25.5mm) steel bar. All the samples were ground down to 1200 grit SiC paper, polished to an average surface roughness of Ra<0.02 μm, ultrasonically cleaned in acetone for 10 min and finally dried with flowing hot air.

2.2 Plasma surface treatment

A newly developed triple-glow plasma (TGP) facility was employed for alloying 316 austenitic stainless steel surfaces simultaneously with the substitutional element silver (Ag) and the interstitial element nitrogen (N). As schematically shown in Figure 1, the earthed furnace wall serves as the anode, both the stainless steel screen and Ag plate were powered by DC source S1 with the same bias, and the samples were powered by DC source S2. The plasma co-alloying treatments were carried out at 420°C for 10h in a gas mixture of $75\%H_2 + 25\%N_2$ with a work pressure of 1 mbar (100Pa). The voltage for S1 and S2 were 500V and 240V, respectively. Whilst the distance between the samples and the metal screen (D1) was maintained at 20mm, the distance between the metal screen and the silver plate (D1) varied from 10mm (AgSS10) to 20mm (AgSS20). The sample code and the treatment conditions are summarised in Table 1.

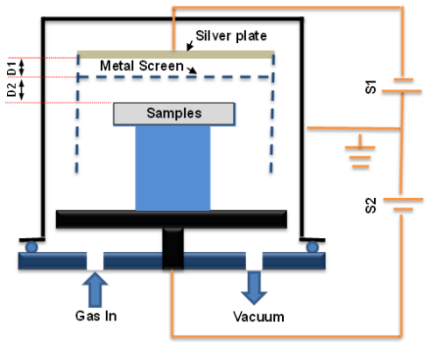

Figure 1 A schematic of triple-glow plasma equipment

Table 1 The sample code and treatment conditions

Samples	S1		S2		D1(mm)	D2(mm)
	Voltage (V)	Current (A)	Voltage (V)	Current (A)		
Untreated	-	-	-	-	-	-
AgSS10	500	0.7	240	0.2	10	20
AgSS20	500	0.7	240	0.2	20	20

2.3 Surface characterisation

The surface morphology and cross-section microstructure of plasma treated surface layers were observed using an Oxford JEOL 7000 scanning electron microscope (SEM). The Ag distribution on the surface was detected by energy-dispersive spectroscopy (EDS) equipped on the Oxford JEOL 7000. The composition depth profiles were measured using glow discharge optical emission spectroscopy (GDOES) in a SPECTRUMA GDA650 spectrometer. The phase constituents of the alloyed surface were analysed using the X'Pert Philips XRD instrument with Cu Kα radiation.

The surface hardness of plasma treated as well as untreated samples was measured using the Mitutoyo MVK-H1 micro-hardness tester with a Vickers indenter at a load of 50 gf. Reciprocating wear tests under a load of 5 N at a frequency of 1 Hz for 1000 cycles against an 8mm alumina ball were conducted to evaluate the tribological properties of the plasma alloyed surfaces using Phoenix Tribology TE79 Multi-axis Tribometer. The wear track profiles were measured using the Ambios XP-200 profilometer and the wear volume and wear rate were calculated based on the measured cross-sectional profiles. The wear tracks were observed using JEOL JSM 6060 SEM equipped with an EDS.

2.4 Corrosion testing

Electrochemical corrosion tests were performed with a Gamry instruments (US) using the standard three-electrode configuration, with a platinum coated rod as a counter electrode, a saturated calomel electrode as a reference electrode and the sample as a working electrode. A circular area of 50.27 mm^2 of surface was exposed to the corrosive solution for every sample. Prior to measurement, the samples were immersed in the solution for 1h to obtain a stable open circuit potential (OCP). The potentiodynamic polarization tests were conducted in 300ml of full strength Ringers solution at a temperature of about 37°C. The sweep was performed at a constant scanning rate of 1mV/s with a

period between -0.3V vs EOCP and 1.5V vs EREF. The morphology after corrosion test was examined using a SEM machine mentioned above.

2.5 Antibacterial testing

Antibacterial activities of plasma treated and untreated stainless steel surfaces were tested under a standard method based on the Japanese JIS2801:2000 spread plate method [20]. The untreated stainless steel samples were used as controls for the Ag-N co-alloyed layers. Gram-positive Staphylococcus aureus (S. aureus) were selected as test bacteria. The bacteria were cultured overnight on tryptic soya broth (TSB) and then serially diluted in TSB to an optical density OD_{600nm} of 0.05, which has been previously shown to be equivalent to 10^7 cells/ml. The stainless steel samples were sterilised by autoclaving and then placed on sterile filter papers saturated with distilled water inside sterile 90 mm diameter Petri dishes to maintain ambient humidity. Fifty microlitres of diluted bacterial suspension was pipetted onto each sample surface, which was then covered with a sterile glass cover slip in order to maintain the same contact area of suspension on each tested surface. All Petri dishes were incubated at room temperature for 12 h. After the designated time the whole sample was transferred to 10 ml of sterile phosphate-buffered saline (PBS) in a sterile container. The contents were vortex mixed for 10 seconds to dislodge the coverslips and suspend the surviving bacteria in the PBS. Serial dilutions of the bacterial suspension were made and 100 µl aliquots of each dilution pipetted onto TSA plates, which were incubated overnight at 37 °C. The number of colony forming units (CFU) resulting from the growth of viable bacterial at 37 °C after 24 h represents the initial viability of bacteria that survived in the suspension. The percentage reduction was calculated using the following equation:

$$Reduction\ (\%) = \frac{N_0 - N_t}{N_0} \times 100\%$$

where N_t and N_0 represent the average CFU/ml for a treat sample after the contact time 't' (t=12h in this study) and at 0 h, respectively. Three specimens of each test material and the controls were analysed and three plates were spread from the PBS suspension resulting from each sample. Results are expressed as means ± SD of the measurements.

3 Results

3.1 Microstructure and hardness

The surface morphology of the plasma co-alloyed AgSS10 (Fig.2a) and AgSS20 (Fig.2a) samples is very similar although the former seems slightly more compact, smoother and finer than the latter. EDX analysis revealed that Ag was distributed uniformly across the whole surface for the both samples. The average silver content in the surface was measured to be about 50 % and 42 % for AgSS10 and AgSS20 respectively, which is much higher than that generated by active-screen plasma technology. This also indicated that the surface Ag content decreased with increasing the distance between the Ag plate and the stainless steel screen lid used for the triple-glow plasma treatments.

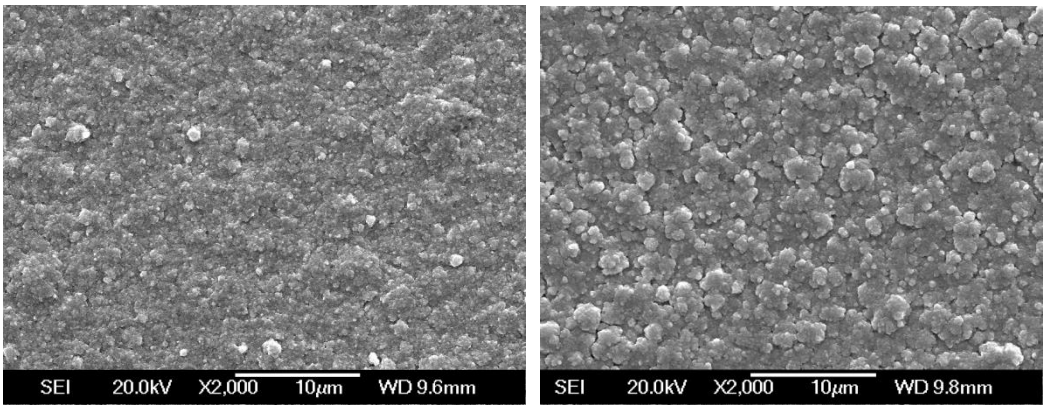

(a) (b)

Figure 2 Surface morphology of plasma co-alloyed (a) AgSS10 and (b) AgSS20

It can be seen from the XRD patterns shown in Figure 2 that both the Ag/N co-alloyed surfaces predominately consisted of Ag and S-phase (i.e. N supersaturated expanded austenite) [21]. It was noted that the intensity of Ag peaks decreased but the S-phase peaks increased when the distance between the Ag plate and the steel lid (D2) increased from 10mm for AgSS10 to 20mm for AgSS20.

Further chemical analysis by GDOES (Figure 3) revealed that a Ag plateau below the surface with an average silver content of about 25 wt% was formed during the Ag/N co-allying process for both samples; the depth of this Ag-enriched layer formed on AgSS10 (about 4μm) is twice that formed on AgSS20 (about 2 μm). Then, the Ag content dropped rapidly to zero where Fe, Cr and Ni reached to the value for the bulk material. On the other hand, N decreased quickly to about 10% within the Ag enriched layer before it decreased gradually to a depth of around 10 μm.

The SEM images taken from the cross-section of Ag/N co-alloyed AgSS10 and AgSS20 samples showed a two-layer structure: a thin surface layer followed by a thick subsurface layer (Figure 5). It can also be seen from Figure 5 that although the total thickness of the treated surface is slightly thicker on AgSS10 than on AgSS20, the top layer formed on the former is much thicker than that formed on the latter.

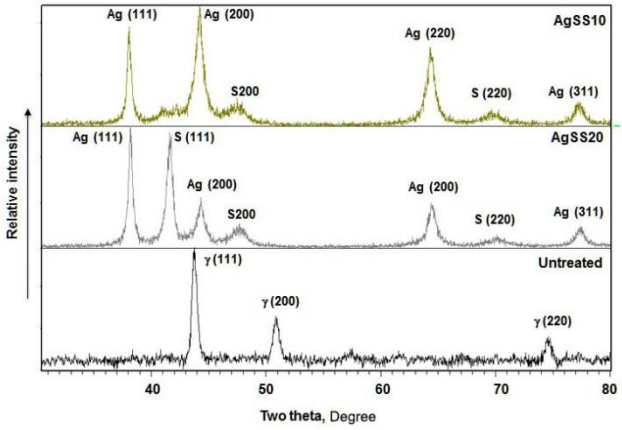

Figure 3 XRD diffraction patterns for Ag/N co-alloyed AgSS10 and AgSS20 surfaces

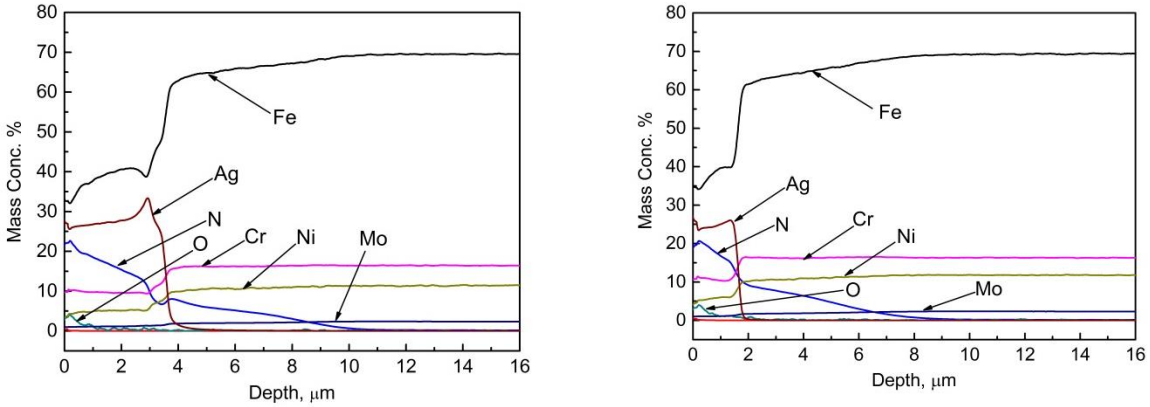

(a) (b)

Figure 4 GDOES charts for (a) AgSS10 and (b) AgSS20

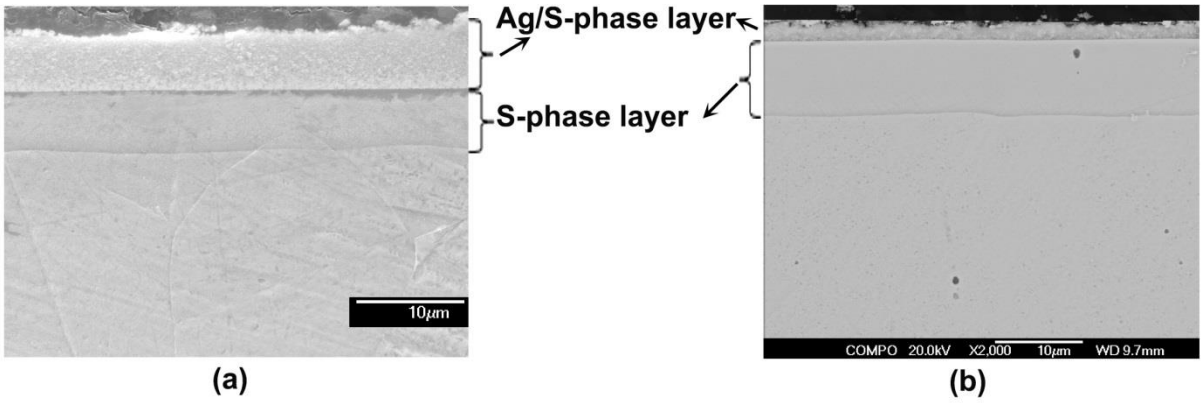

Figure 5 Cross-sectional SEM micrographs of (a) AgSS10 and (b) AgSS20

It can be deduced based on the above XRD, GDOES and SEM micrograph in conjunction with the principle of the triple-glow plasma technology that the Ag/N co-alloyed surface cases were composed of a thin top layer (2-4 μm) containing about 20-25% Ag embedded in N supersaturated austenite (i.e. S-phase) followed by a relatively thick (5.5-80 μm) S-phase layer. It is clear from Figure 5 that the thickness of the top Ag/S-phase layer formed on AgSS10 sample is close to 4 μm while the top deposition layer formed on AgSS20 is about half of that. This is mainly due to the fact that the Ag plate and the stainless steel lid formed a hollow cathode and the discharge is closely related to the distance between them (D2) under a constant working pressure. The discharge became stronger with decreasing the distance D2 and hence more Ag atoms from the Ag plate cathode were sputtered and co-deposited with 316 material on the sample surface to form a thicker co-deposition layer.

This is supported by the measured surface hardness shown in Figure 6. The hardness measurement results have indicated that although the surface hardness of Ag/N co-alloyed AgSS10 (580HV0.05) is more than twice as hard as that of the untreated materials (250HV0.05), it is still much softer than Ag/N co-alloyed AgSS20 (900HV0.05) due to the high Ag content in the top deposition layer. The thicker S-phase layer formed on AgSS20 than on AgSS10 is also related to the lower Ag content in the former than in the latter since it is know that Ni, Cu and Ag will retard the inward diffusion of N during diffusion treatment [22].

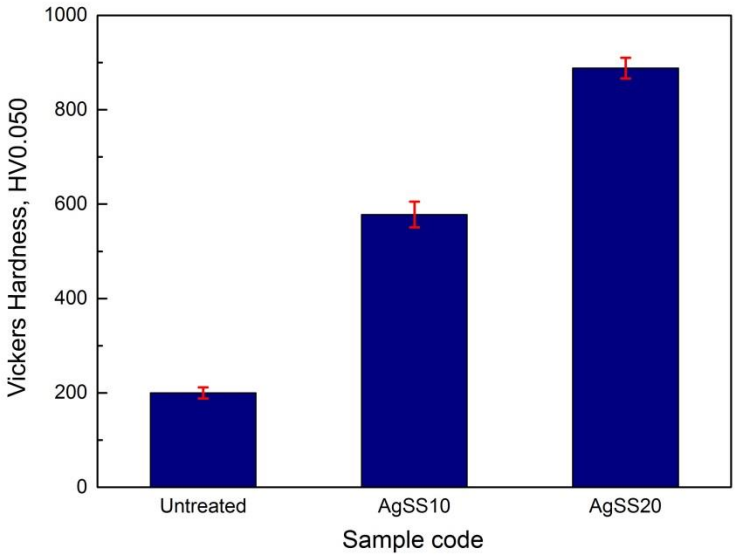

Figure 6 Surface hardness of N/Ag co-alloyed and untreated samples

3.2 Corrosion properties

The corrosion behaviour of the Ag/N co-alloyed layers and untreated surface in the full strength Ringers solution was tested by electrochemical polarization and the results are shown in Figure 7. It can be seen that both of the Ag/N co-alloyed surfaces showed a more positive corrosion potential than the untreated 316 ASS. The results of the quantitative analysis of the polarization curves are summarised in Table 2. It revealed that the corrosion potential (E_{corr}) was reduced from -274 mV vs SCE for the untreated 316 to -243 mV vs SCE for AgSS10 and -189 mV vs SCE for AgSS20. The corrosion current density (I_{corr}) and corrosion rate of AgSS20 is almost the same as that of the untreated material but AgSS10 showed increased I_{corr} and corrosion rate as compared with untreated surface.

It is also revealed in Figure 7 that severe pitting corrosion occurred to the untreated surface when the applied potential reached about 250mV vs SCE as evidenced by the steep increase of the current density. The current density reached as high as 10mA/cm^2 under an applied potential of 1000 mV vs SCE. Although rapid increase in current density was also observed for the Ag/N co-alloyed surfaces, it seems that the pitting process was stopped as evidenced by a plateau towards the end of the polarization curves.

Post-test SEM observations proved that the corroded surface of the untreated sample revealed many deep pits (Figure 8a) but only shallow corroded areas were observed from the Ag/N co-alloyed surface after test (Figure 8b). This implied that corrosion may have occurred to the surface deposition layer but the underlying S-phase layer remained almost fully intact, therefore demonstrating even better corrosion resistance than the untreated 316 ASS [21]. Clearly, the Ag/N co-alloyed AgSS20 sample possessed improved corrosion behaviour than the untreated material.

Table 2 Anodic polarisation corrosion results for the untreated and Ag/N co-alloyed samples

Samples	**E_{corr}(mV)**	**I_{corr}(×10^{-5}mA/cm^2)**	**Corrosion rate (×10^{-2}mpy)**
Untreated	-274	8.9	8.1
AgSS10	-243	124	112.9
AgSS20	-189	9.0	8.2

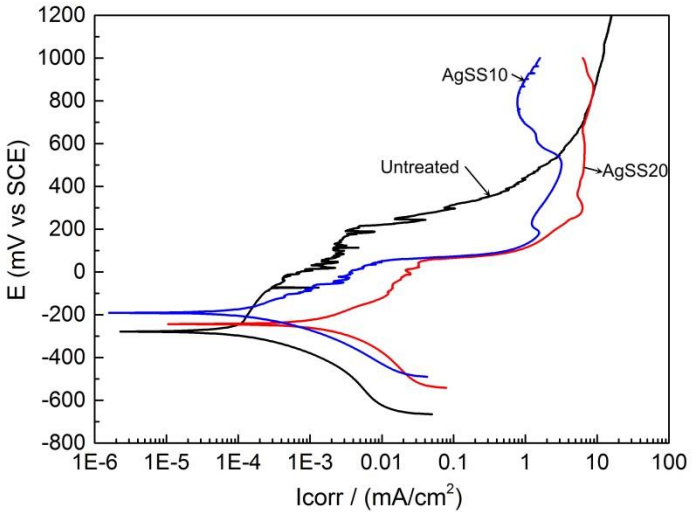

Figure 7 Anodic polarisation curves for untreated and Ag/N co-alloyed samples

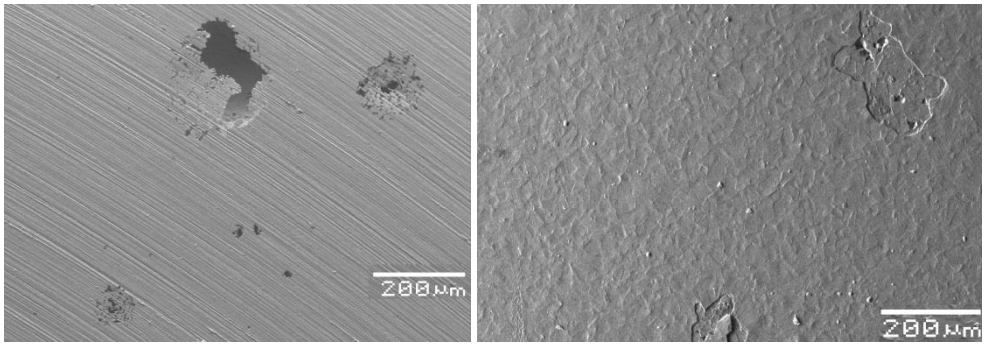

(a) (b)

Figure 8 Surface images after corrosion test for (a) untreated and (b) AgSS20 samples

3.3 Antibacterial behaviour

The antibacterial properties of Ag/N co-alloyed layers and untreated ASS controls were evaluated with Gram positive bacteria (*S.aureus*) and using a contact time of 12h. The spread results of viable following testing are shown in Figure 9. It can be clearly seen that the spread plate of the untreated 316 surface was almost completely covered by bacterial colonies (Figure 9a). In contrast, the numder of colonies remaining on the Ag/N co-alloyed 316 plate surface was reduced significantly (Figures 9b and c).

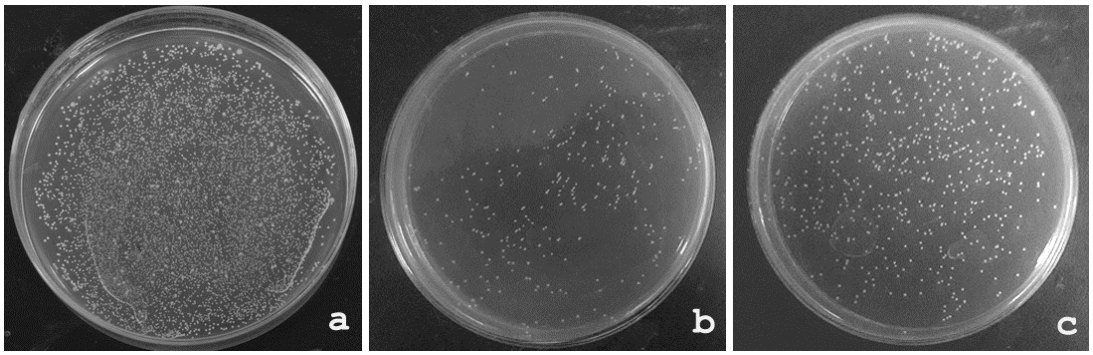

Figure 9 Qualitative spread plates results of viable bacterial number after 12 h contacting with (a) untreated 316 control and Ag/N co-alloyed (b) AgSS10 and (c) AgSS20 samples

The quantitative reduction rate of the bacteria relative to the 316SS control sample was calculated and the results are given in Figure 10. It is evident that the cultures of *S.aureus* were effectively killed by exposure to Ag/N co-alloyed surfaces and the reduction percentage is ~95 and 91% for AgSS10 and AgSS20 samples respectively. As reported above, the surface of AgSS10 samples contained a slightly higher percentage of Ag (about 50%) than that of AgSS20 sample (42%). This suggests that the higher the Ag content the higher the antibacterial efficacy.

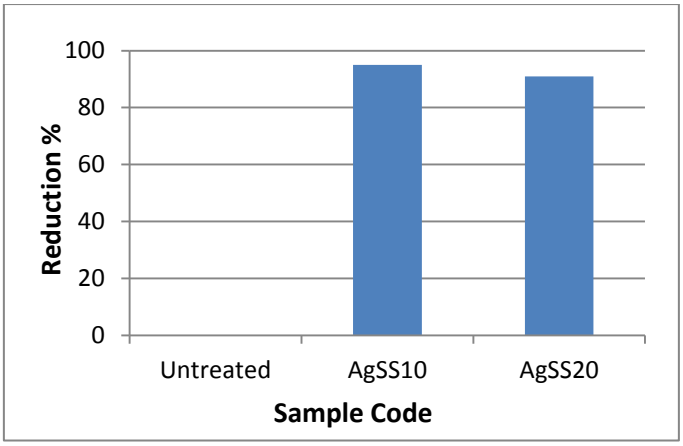

Figure 10 Reduction rate of the number of viable bacteria on Ag/N co-alloyed samples

3.4 Wear resistance and durability

As discussed in the introduction, the most challenging issue for anti-bacterial surfaces is their durability especially under tribological conditions. To this end, the durability of the new Ag/N co-alloyed 316 surfaces were studied using reciprocating sliding against an 8mm alumina ball under a load of 5 N.

Figure 11 summarises the wear factor of the Ag/N co-alloyed 316 surfaces and the untreated material for comparison. As depicted in Figure 11, the novel Ag/N co-alloying treatment can significantly increase the wear resistance of 316 austenitic stainless steel. In particular, the wear rate of the Ag/N co-alloyed layer formed on AgSS20 sample is only about one percent of that for the untreated 316 material.

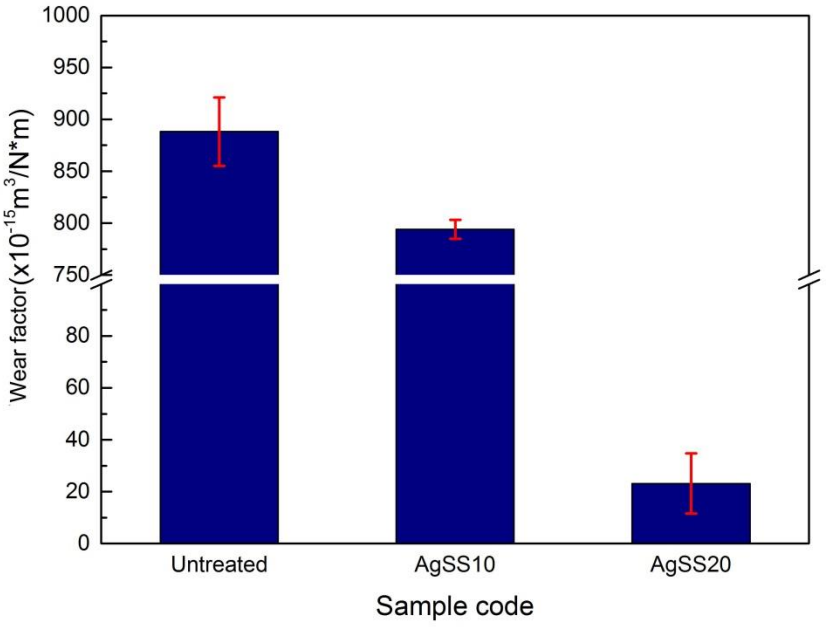

Figure 11 Wear rate of the untreated and Ag/N co-alloyed samples

Detailed post-test studies were carried out to investigate the wear of the Ag/N co-alloyed surfaces. As expected, severe adhesive wear and abrasive wear occurred to the untreated 316 surface mainly due to its low-hardness and high adhesive wear tendency [23].

Figure 12a shows the wear scar formed on the surface of the AgSS10 sample after the wear test with relatively deep and wide parallel wear groves indicative of severe abrasive wear. The EDX spectra taken from the wear track (Figure 12b) showed a very weak Ag peak. This indicates that the Ag rich surface layer formed on AgSS10 was removed by the wear and the weak peak of Ag is most probably from the wear debris embedded in the wear track.

On the other hand, as shown in Figure 12b, although a wear scar was also observed from the tested AgSS20 sample surface, mild abrasive wear occurred to the surface. This is supported by the very strong Ag peak in the EDX spectra taken from the wear track formed on AgSS20 surface (Figure 12d). This significantly increased wear resistance could be attributed to the effectively enhanced surface hardness (900HV0.05) because it is known that abrasive wear resistance of a surface is proportional to its hardness [24]. It is the effectively increased wear resistance that has contributed to the durability of the Ag enriched surface. A few spallations were observed in some localised areas of the wear scar on Ag-SS20, which could be related to the delamination of the deposition layer after many cycles of reciprocating friction and wear.

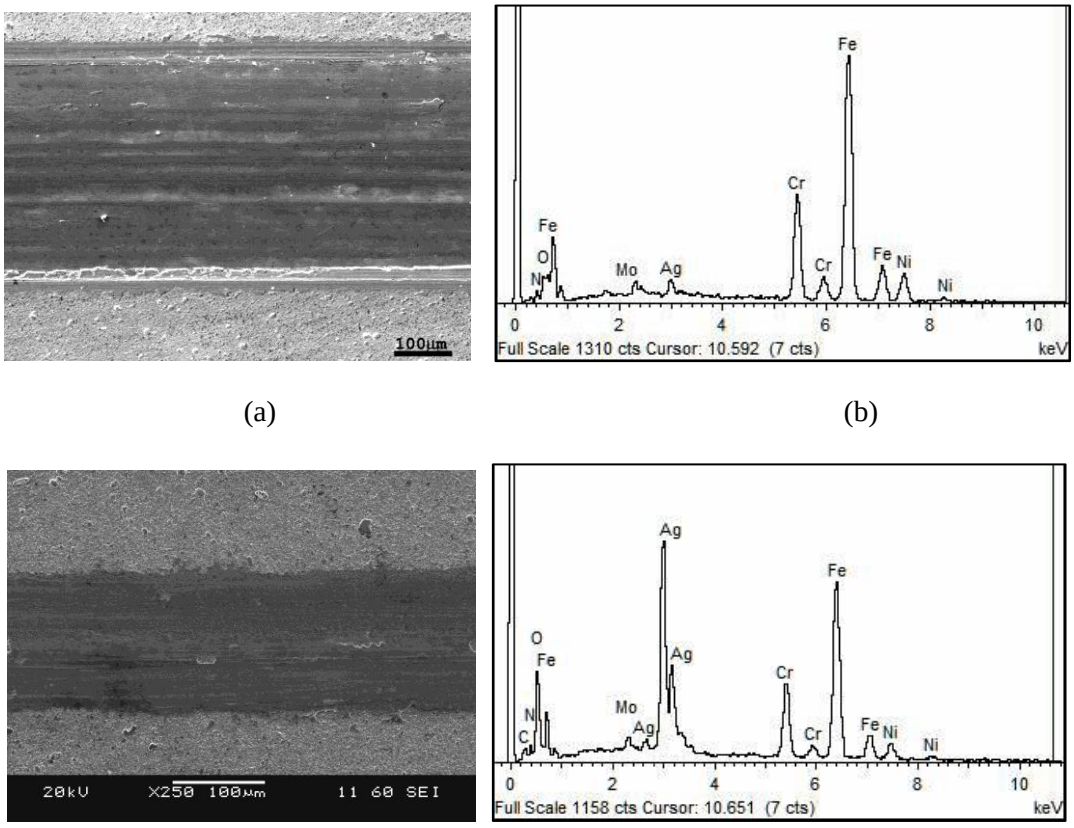

Figure 12 Wear scars on (a) AgSS10 and (c) AgSS20 and EDS spectra taken from the wear track formed on (d) AgSS10 and on (d) AgSS20

4 Discussion

As previously discussed in the Introduction, it has long been a dream for the designers of surgical tools, body implants, hospital equipment and other medical devices to have antibacterial surfaces that meet the ever-increasing demand for combating medical device-associated and hospital-acquired infections [6,9]. To this end, great effort and hence meaningful progress has been made during the past decade to generate anti-bacterial surfaces by silver (Ag) coating [16,25], Ag-doped polymer coatings [26], Ag-DLC [27], Ag-TiO_2 [28] and Ag-Al_2O_3 [29] composite coatings, Ag ion implantation [30] and more recently nano [31] or micro [32] patterning.

Notwithstanding the fact that all these approaches have made progress in generating anti-bacterial surfaces, one of the most challenging issues to be addressed is the durability of the anti-bacterial

surfaces for bio-tribological applications such as surgical and dental tools, internal and external fixation devices and healthcare equipment involving relative movement. This is because Ag-doped polymer coatings are too soft to withstand scratching; the modified surface by Ag implanted and nano/micro patterning surface layers are too thin (<0.5 μm) to survive long-term tribological loading; and the major concerns over Ag-containing composite coatings under tribological application are poor interface bonding and low load bearing capacity when coated on relatively soft austenitic stainless steel surfaces [33]. Failure of such Ag-containing coatings will lead to fast leaching of Ag ions and the resulted detrimental loss of bactericidal properties [9].

In this research, new anti-bacterial stainless steel surfaces have been generated using a novel triple-glow plasma co-alloying technology with both the interstitial element of nitrogen (N) and the substitutional element silver (Ag). As has been shown in Figures 10 and 11, both Ag/N co-alloyed AgSS10 and AgSS20 316 surfaces possess a high anti-bacterial efficacy and a low wear rate when compared with the untreated 316 stainless steel.

As briefly discussed in the Introduction, both surface topography and surface chemistry will influence the bacterial cell attachment, colonisation and invasion. It was found that the roughness of the treated surfaces was increased from about 0.02 to 0.2 μm (Ra). In view of this, the roughness of the untreated surface (i.e. control) was adjusted by grinding using SiC abrasive papers with different grits to match the Ra value for the treated surfaces to avoid the effect of surface roughness. It should be admitted that it is impossible to produce the same surface morphology as for the plasma treated one. Antibacterial testing demonstrated that the AgSS10 surface with a high level of Ag (50 %) exhibited a higher anti-bacterial efficacy than the AgSS20 surface with a relatively low level of Ag (42 %) although both treatments had very similar surface morphologies. Thus, it follows that the anti-bacterial behaviour observed for the TGP treated 316 surfaces is related to the high concentration of Ag introduced into the surface by Ag/N co-alloying. Although it is not fully elucidated, the most convincing mechanism of action is that Ag^+ interacts directly with pathogens by binding to their cellular membranes causing perforations, and subsequent leakage of the pathogen's intracellular substances resulting in cell death [34 35].

The reasons for the significantly increased wear resistance by Ag/N co-alloying could be twofold. Firstly, hardness measurement revealed that the surface hardness of 316 can be increased from about 250HV0.05 for the untreated material to 580 HV0.05 and 900 HV0.05 for AgSS10 and AgSS20, respectively. The increased surface hardness due to the formation of hard S-phase has contributed to the improved wear resistance since it is known that the resistance of a material to abrasive wear is proportion to its hardness. This partially explains the higher wear resistance of AgSS20 relative to AgSS10. Secondly, the formation of the S-phase sublayer (Figure 5) can mechanically support the top Ag rich layer and hence increase the load bearing capacity (LBC) of the Ag/N co-alloyed dual-layered surface system. It is clear from Figures 4 and 5, a thicker S-phase sublayer was formed on AgSS20 than on AgSS10 and hence a better LBC and higher wear resistance is expected from the former than from the latter.

The change of surface topography (Figure 12c) of the wear track and its very small area make it impossible to test again for antibacterial behaviour following wear testing. As has been revealed in Figure 12, the high wear resistance of the antibacterial surface developed from this research on AgSS20 should transform to high durability of the antibacterial effect as the wear track formed on AgSS20 still contained a high level of Ag. It thus follows based on the above discussion on antibacterial efficacy and wear resistance that the antibacterial surface formed by AgSS20 is expected to have good durability with satisfactory anti-bacterial efficacy. The potential of the novel long-lasting anti-bacterial stainless steel surfaces will be explored in future by applying the novel triple-glow plasma co-alloying technology to austenitic stainless steel external fixation pins and some surgical tools.

5 Summary and Conclusions

A newly developed triple-glow plasma technology has been developed to alloy austenitic stainless steel surfaces simultaneously with both the substitutional element nitrogen and the substitutional element silver (i.e. Ag/N co-alloying). A dual layered surface system consisting of a thin (a few microns) Ag doped S-phase (nitrogen supersaturated austenite) top layer and a relatively thick (~10 microns) S-phase sublayer can be formed on AISI 316 steel at 420℃ with a sample bias of 240V in a

gas mixture of $25N_2$ + $75\%H_2$. The surface layer structure is highly dependent on the distance between the Ag cathode and the steel mesh cathode. When the distance between the Ag cathode and the steel mesh cathode increased from 10mm for AgSS10 sample to 20mm for AgSS20 sample, the thickness of the top Ag rich layer decreased from 4.5 to 2 μm and the surface Ag content reduced from 50% to 42%.

The Ag/N co-alloyed surfaces possess high antibacterial efficacy mainly due to the high amount of Ag (42-50%) introduced into the S-phase matrix formed on the top layer, which denature the thiol groups of bacterial proteins and enzymes; the surface hardness of 316SS is increased from 250 for the untreated material to 580 and 900HV0.05 for AgSS10 and AgSS20 respectively; and the wear factor is reduced from 890 for the untreated material to 250 and 23 $x10^{-15}$ $m^3N^{-1}m^{-1}$ for AgSS10 and AgSS20 respectively. The wear track formed on AgSS20 surface still contained a very high level of Ag and hence long-lasting antibacterial efficacy is expected.

The optimal AgSS20 treatment can generate multi-functional stainless steel surfaces with a high hardness, a high anti-bacterial efficacy, slightly enhanced or at least maintained corrosion resistance in the Ringers solution and excellent wear resistance and hence long durability, which are expected to have great potential for future long-lasting antibacterial stainless steel surfaces for medical devices.

Acknowledgement

This research was mainly supported by an EC Marie Curie International Incoming Fellowship (PIIF-GA-2012-327750) together with the support from EPSRC UK (EP/J018252) and Shanxi Scholarship Council of China (2016-025).

References

1 Davis JR. Handbook of Materials for Medical Devices. ASM International:Materials Park; 2003, p.27.
2 Lipscomb IP et al. Are surgical stainless steel wires used for intracranial implantation of PrPsc a good model of iatrogenic transmission from contaminated surgical stainless steel instruments after cleaning? *Journal of Hospital Infection*, 2006; **64**: 339-343.
3 Massè A, Bruno A, Bosetti M, et al. Prevention of pin track infection in external fixation with silver coated pins: clinical and microbiological results. J Biomed Mater Res. 2000; **53**: 600-604.
4 Wickens DJ, West G, Kelly PJ, at al. Antimicrobial activity of nanocomposite zirconium nitride/silver coatings to combat external bone fixation pin infections, Int J Artif Organs, 2012;**35**: 817-825.
5 Bright KR et al. Journal of Hospital Infection. 2001; **52:** 307-309.
6 Weber DJ, Rutala W.A. Self-disinfecting surfaces: Review of current methodologies and future prospects. American Journal of Infection Control. 2013; **41:** S31-S35.
7 Aston University [internet]. Birmingham UK: [cited 2016 Dec 29]. Available from: http://www.aston.ac.uk/research/case-studies/mrsa/
8 The House of Commons' Committee on Public Accounts (Copper Development Association, 2005)
9 Campoccia D, Montanaro L, Arciola CR. A review of the biomaterials technologies for infection-resistant surfaces,.Biomaterials.2013; **34;** 8533-8554.
10 Weber D J and Rutala W A, Self-disinfecting surfaces: Review of current methodologies and future prospects. American Journal of Infection Control. 2013; **41**: S31-S35.
11 Lorenzetti M, Dogša I, Stošicki T, et al. The influence of surface modification on bacterial adhesion to titanium-based substrates. Applied Materials & Interfaces. 2014; **7**: 1644-1651.
12 Chung KK, Schumacher JF, Sampson EM, et al.. Impact of engineered surface microtopography on biofilm formation of Staphylococcus aureus. Biointerphases. 2007; **2**: 89-94.
13 Feng QL et al. A mechanistic study of the antibacterial effect of silver ions on Escherichia coli and Staphylococcus aureus. Journal of Biomaterials Research. 2000; **52:** 662-668.
14 Prokopovich P, Kobrick M, Brousseau E et al. Potent antimicrobial activity of bone cement encapsulating silver nanoparticles capped with oleic acid. J Biomed Mater Res B Appl Biomater.2015; **103:**273-81.
15 Toy LW, Macera L. Evidence-based review of silver dressing use on chronic wounds. J Am Acad Nurse Practitioners. 2011; **23:** 183-92.
16 Furkert FH, Sörensen JH, Arnoldi J et al. Antimicrobial efficacy of surface-coated external fixation pins. Curr Microbiol. 2011; **62;**1743–1751.
17 Dong YC, Li X, Simon R and Dong H.The generation of wear-resistant antimicrobial stainless steel surfaces by active screen plasma alloying with N and nanocrystalline Ag. Journal of Biomedical Materials Research Part B. 2010; 93B:185-193.
18 Dong Y C, Li X, Tian L et al. Towards long-lasting antibacterial stainless steel surfaces by combining double glow plasma silvering with active screen plasma nitriding. Acta Biomaterialia. 2011; 7: 447-457.
19 Dong H, Li X, Dong Y, Tian L. Long-lasting antibacterial metallic surfaces and methods for their production. EP 2870269 A2 (patent number WO2014006390).
20 Suzuki S, Imai S, Kourai H. Background and evidence leading to the establishment of the JIS standard for antimicrobial products. Biocontrol Sci, 2006; **11:**135–145.
21 Dong H. S-phase surface engineering of Fe-Cr, Co-Cr and Ni-Cr alloys, International Materials Review. 2010; **55**:65-98.
22 Cahn RW. Physical Metallurgy 1. 4th ed. Elsevier. 1996, p1355.
23 Smith AF, The sliding wear of 316 stainless steel in air in the temperature range 20–500°C. Tribology International. 1985; **18:** 35–43.
24 Bressan J D, Daros D P, Sokolowski A, et al. Influence of hardness on the wear resistance of 17-4 PH stainless steel evaluated by the pin-on-disc testing. Journal of Materials Processing Technology. 2008; **205(1)**: 353-359.
25 Calling CA, Goll G, Seligson D et al. Pin tract infection: silver vs uncoated pins. ProQuest Nursing & Allied Health Source. 1994;**17**(No. 5):445-448.
26 Cowan MM et al. Antimicrobial efficacy of a silver-zeolite matrix coating on stainless steel. Journal of Industrial Microbiology and Biotechnology, 2003; **30:**102-106.
27 Marciano FR et al. Antibacterial activity of DLC and Ag-DLC films produced by PECVD technique. Diamond and Diamond Related Materials. 2009; **18:**1010-1014.
28 Li B et al. Preparation and anti-bacterial properties of plasma sprayed nano-titania/silver coatings. Materials Chemistry and Physics. 2009; **118:** 99-104.
29 Gao J, Li C, Zhou J, Lu L et al. Plasma sprayed alumina–nanosilver antibacterial coatings. RSC Advance. 2015; **5:** 20357-20364.
30 Wan YZ, Raman S, He F et al, Surface modification of medical metals by ion implantation of silver and copper, Vacuum.2007; 81:1114–1118.

31 Bagherifard S, Hickey DJ, Luca AC et al.The influence of nanostructured features on bacterial adhesion and bone cell functions on severely shot peened 316L stainless steel. Biomaterials. 2015; **73:** 185-197.
32 Valle J, Burgui S, Langheinrich D et al. Evaluation of surafce microtopography engineered by direct laser interference for bacterial anti-biofouling. Macromolecular Bioscience. 2015; **15:** 1060-1069.
33 Luo X, Li X, Design and characterisation of a new duplex surface system based on S-phase hardening and carbon-based coating for ASTM F1537 Co–Cr–Mo alloy, Applied Surface Science. 2014;**292:**336-344.
34 Knetsch M L W and Koole L H, New strategies in the development of antimicrobial coatings: The examples of increasing usage of silver and silver nanoparticles. Polymers. 2011; **3**:340-366.
35 Lara H, Garza-Trevino E, Ixtepan-Turrent L, et al. Silver nanoparticles are broad-spectrum bactericidal and virucidal compounds. Journal of Nanobiotechnology. 2011; **9**:30.